Cationic Poly-L-lysine Dendrimer Complexes Doxorubicin and Delays Tumor Growth *in Vitro* and *in Vivo*

Khuloud T. Al-Jamal,[†,‡,*] Wafa' T. Al-Jamal,[†,‡] Julie T.-W. Wang,[‡] Noelia Rubio,[‡] Joanna Buddle,[§] David Gathercole,[⊥] Mire Zloh,[⊥,∥] and Kostas Kostarelos[†,*]

[†]Nanomedicine Laboratory, Centre for Drug Delivery Research, UCL School of Pharmacy, University College London, 29-39 Brunswick Square, London WC1N 1AX, United Kingdom, [‡]Institute of Pharmaceutical Sciences, King's College London, Franklin-Wilkins Building, 150 Stamford Street, London SE1 9NH, United Kingdom, [§]Flow cytometry unit, UCL Institute of Child Health, 30 Guilford Street, London WC1N 1EH, United Kingdom, [⊥]UCL School of Pharmacy, University College London, 29-39 Brunswick Square, London WC1N 1AX, United Kingdom, and [∥]University of Hertfordshire, Department of Pharmacy, College Lane, Hatfield, Hertfordshire AL10 9AB, United Kingdom

ABSTRACT We report in this study the complexation of the chemotherapeutic drug doxorubicin (DOX) with the novel sixth-generation cationic poly-L-lysine dendrimer (DM) (MW 8149 kDa), which we previously reported to exhibit systemic antiangiogenic activity in tumor-bearing mice. DOX—DM complexation was confirmed by florescence polarization measurement, proton nuclear magnetic resonance spectroscopy, and molecular modeling. Enhanced penetration of DOX—DM (at 1:10 molar ratio), compared to the free DOX, into prostate 3D multicellular tumor spheroids (MTS) was confirmed by confocal laser scanning microscopy. Furthermore, DOX—DM complexes achieved a significantly higher cytotoxicity in DU145 MTS system compared to the free drug, as shown by growth delay curves. Incubation of MTS with low DOX concentration (1 μM) complexed with DM led to a significant delay in MTS growth compared to untreated MTS or MTS treated with free DOX. DOX—DM complex retention was also achieved in a Calu-6 lung cancer xenograft model in tumor-bearing mice, as shown by live whole animal fluorescence imaging. Therapeutic experiments in B16F10 tumor bearing mice have shown enhanced therapeutic efficacy of DOX when complexed to DM. This study suggests that the cationic poly-L-lysine DM molecules studied here could, in addition to their systemic antiangiogenic property, complex chemotherapeutic drugs such as DOX and improve their accumulation and cytotoxicity into MTS and solid tumors *in vivo*. Such an approach offers new capabilities for the design of combinatory antiangiogenic/anticancer therapeutics.

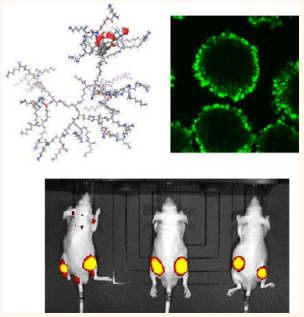

KEYWORDS: cancer · growth delay · penetration · uptake · retention · fluorescence · solid tumor

Dendrimers are three-dimensional nanocontainers synthesized in a stepwise manner by attaching branching units to an emanating core.[1] Their size, molecular weight, and surface functionalities can be easily controlled.[1] Dendrimers have been proposed as delivery agents for chemotherapeutic drugs to solid tumors. Malik *et al.*[2] showed that conjugates of cisplatin with the negatively charged PEGylated generation 4 polyamidoamine (PAMAM) dendrimer exhibited antitumor activity against B16F10 solid tumors. Methotrexate (MTX) conjugated to PEGylated poly-L-lysine dendrimers (G_5, PEG1100) has also shown to accumulate in solid Walker 256 and HT1080 tumors in rats and mice.[3] Recently, a study by Fox *et al.*[4] reported therapeutic efficacy of PEGylated poly(L-lysine) dendrimer—camptothecin conjugates in C26 and HT-29 tumor models.

We have reported recently and for the first time the intrinsic antiangiogenic activity of cationic sixth-generation poly-L-lysine (PLL) dendrimer (MW 8149 Da) using a panel of *in vitro* and *in vivo* assays.[5] Intravenous administration of only two doses at 50 mg/kg PLL dendrimer resulted in persistent accumulation in solid tumor sites (B16F10 model), reduction in vascularization, extensive apoptosis/necrosis within the tumor tissue, and statistically significant but moderate reduction in tumor volume, in the absence of any remarkable histological or physiological abnormality in nontumor tissues such as liver and kidneys. The dendrimer showed therapeutic efficacy comparable to the commercially available anti-VEGF antibody bevacizumab (Avastin) in delaying the growth of a subcutaneous B16F10 melanoma tumor model. Several studies have indicated that the addition of antiangiogenic therapeutics along with chemotherapy or radiotherapy[6] can synergistically improve tumor responses to treatment.

* Address correspondence to kostas.kostarelos@pharmacy.ac.uk; khuloud.al-jamal@kcl.ac.uk.

Received for review June 22, 2012 and accepted February 14, 2013.

Published online March 07, 2013
10.1021/nn305860k

Doxorubicin (DOX) is a slightly basic anticancer agent widely used in the treatment of human cancer with drawbacks such as poor water solubility and poor penetration *in vitro*[7−9] and *in vivo*,[10−12] posing a major limitation. The present study is based on the hypothesis that the antiangiogenic sixth-generation cationic poly-L-lysine dendrimers Gly-$Lys_{63}(NH_2)_{64}$ (DM)[5,13] have the capability to bind noncovalently the anticancer drug DOX and enhance its penetration into a 2D planner culture model, multicellular tumor spheroids (MTS), and *in vivo* solid tumors.

We tested the hypothesis by assessing the interaction between DM and DOX using florescence polarization (FP) and nuclear magnetic resonance (NMR) spectroscopy and support it by molecular modeling. Penetration of DOX and DOX−DM complexes into MTS was assessed by optical slicing using confocal laser scanning microscopy (CLSM) and measuring the fluorescence of DOX as a function of distance from the outer MTS rim. The biological activity of DOX−DM complexes was assessed *in vitro* by measuring the degree of necrosis/apoptosis of the DU145 monolayer and MTS using Annexin V-FITC and propidium iodide (PI) staining and monitoring MTS growth delay. Complexation of DOX to DM was concluded to lead to enhancement in DOX penetration into MTS with significant MTS growth delay in comparison to the free drug. *In vivo* therapeutic experiments reported significant improvement in tumor growth delay and survival rate compared to the free drug at doses as low as 0.5 mg/kg. Such results suggest the potential of dendrimer−drug complexes as synergistic antiangiogenic/anticancer therapeutics to be translated clinically.

RESULTS

Fluorescence Characterization of DOX−DM Complexes. Cationic sixth-generation poly-L-lysine dendrimer used in this study exhibited a diameter of 6.36 ± 0.34 nm and a zeta potential of 50 ± 2 mV, as previously described.[5] Complexation of DM with DOX had no effect on DM size or zeta potential (Supplementary Table S1). DOX is a fluorescent molecule with excitation and emission wavelengths of 470 and 570 nm, respectively. To investigate whether complexation to DM would affect the spectroscopic properties of DOX, the latter was complexed to DM at different molar ratios, and the fluorescence properties were studied using spectrofluorometry. Supplementary Figure S1 represents the fluorescence characteristics of DOX−DM complexes. The results showed that complexation of DOX to DM, at all molar ratios, did not alter the DOX emission maximum (Supplementary Figure S1). More interestingly, there was a slight but not significant increase in DOX fluorescence intensity upon complexation (<10%) (Supplementary Figure S1) . The slight increase in DOX fluorescence was likely a result of improved DOX solubility upon complexation, as shown by NMR studies below.

Fluorescence polarization was also employed in this study to assess the interaction between DOX and DM. Windsor and Tinker[14] has previously reported the use of fluorescence polarization changes to probe the interactions between DNA and DOX. This technique measures changes in the orientation of plane-polarized light brought about by a fluorophore, in this case DOX, that undergoes significant molecular motion during its fluorescence lifetime. Our results showed a concentration-dependent increase in FP from 0.13 to 0.25 at 1:0 and 1:20 DOX:DM molar ratio (Supplementary Figure S1), respectively, indicating some kind of interactions occurring. However, the type of interaction (*i.e.*, physical entrapment, hydrogen-bonding, and/or hydrophobic−hydrophobic interactions) could not be concluded using this technique.

NMR Spectroscopy and Molecular Modeling of DOX−DM Complexes. ^{1}H NMR spectroscopy is one technique that can be used to determine if there are any changes in the protons' local environment. A set of 1D ^{1}H NMR spectra were acquired at 298 K for DOX and its complex. A comparison between the spectra revealed some differences in chemical shift values for some of the peaks. The NMR spectra of DOX, DM, and their mixture are shown in Figure 1A and B. A minor downfield chemical shift was observed for CH_2 peaks belonging to γ, δ, and ε methylene groups of the lysine in the DM[15] with chemical shift values of 1.4, 17, and 3.0 ppm, respectively. The change in chemical shift of the methylene groups was about 0.6 Hz, and that might not seem significant. However, this small increase of chemical shift could be due to the large excess of DM used and the fact that the peak positions are just an average of shifts of all the branches that could or could not interact with DOX molecules. The observation that Hα proton chemical shifts have not changed at all indicates that the chemical shift changes seen were not a result of conformational changes of the DM molecule, but are more likely to occur as a result of complexation with DOX molecules.

The 1D ^{1}H NMR spectrum of DOX has also revealed some changes in its proton environment. Figure 1B showed a significant change in the position and shape of DOX aromatic peaks when complexed with DM, which is also indicative of the interactions between the two chemical species. There was a change in the chemical shifts of the three aromatic protons in DOX molecule from 7.81, 7.75, and 7.53 ppm to 7.84, 7.85, and 7.57 ppm, respectively, upon complexation. The remaining protons of DOX have shown only minimal shift (2−4 Hz) compared to 17 Hz in the case of aromatic protons. Such a change in chemical shift was not a result of changes in the pH before and after complexation, as the pH of both solutions was checked and found to be comparable (pH of 6.11 for DOX *versus* 6.18 for DOX−DM). Another important finding was the significant improvement in the signal-to-noise ratio of

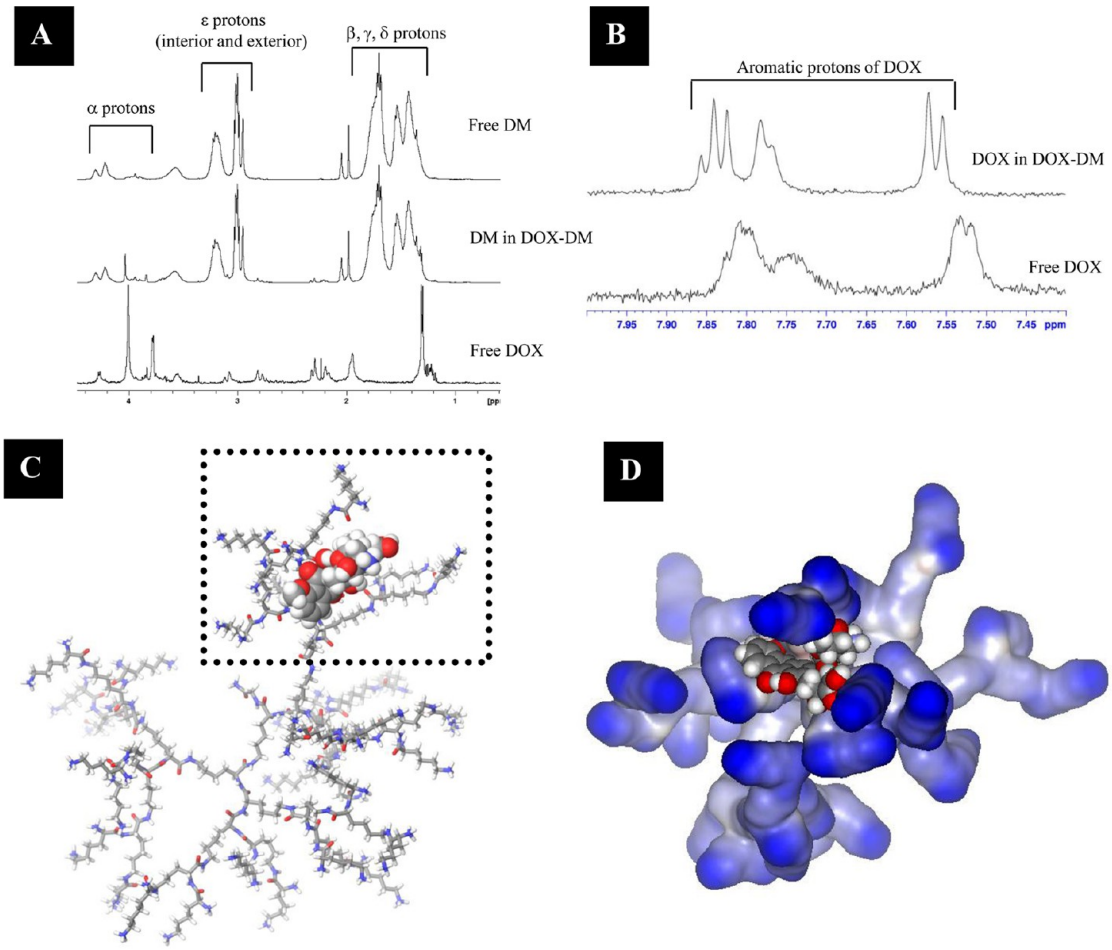

Figure 1. Assessment of DOX:DM complexation by NMR spectroscopy and molecular modeling. Expansions of the 1D ^{1}H NMR spectra of (A) free DM (bottom) and complexed DM; (B) free DOX (bottom) and complexed DOX. (C) The lowest energy conformation of the DOX−DM complex, generated using MCMM conformational search. (C and D) The DOX−DM complex extracted from a snapshot of the molecular dynamics simulation of the system with explicit water. DM is shown in CPK representation represented as sticks in (c) and as a surface with interpolated charges in (d). The positively charged groups are shown in blue on the molecular surfaces.

DOX when complexed with DM (Figure 1B), which could be a result of reduced self-association of DOX upon complexation.

Such findings by NMR spectroscopy were supported by molecular modeling of the DOX−DM complex. A set of DOX−DM conformations was generated using the MacroModel V9.11 suite of software programs. Monte Carlo Multiple Minimum (MCMM) conformational searching with 5000 steps was employed to find the lowest energy structures for the complex starting from two different configurations of a substructure consisting of one DM branch and one DOX molecule. The combination of the OLSA2005 force field and generalized Born/surface area continuum (GB/SA) implicit representation of water as the solvent was used. The lowest energy conformer of the complex is shown in Figure 1C. Although it might be perceived that there are unfavorable repulsing interactions between the NH_3^+ group in both DOX and the DM branches, molecular modeling revealed the possibility of hydrogen bond formation between the amino group of the DM and the carbonyl group or hydroxyl groups of DOX. Furthermore, we have positioned DOX molecules 5 Å away from the DM and confirmed the complex formation between DOX and DM by molecular dynamics simulation in the presence of explicit water molecules. The complex formation was observed by monitoring the number of intermolecular contacts (Supplementary Figure S2A). The DOX molecules were establishing favorable interactions after 1.5 ns simulation at 300 K. The DM−DOX interactions were further enhanced by allowing the full flexibility of DM during the simulation (Figure 1D). To further investigate the stability of the complex, the lowest energy conformation was subjected to 5000 ps molecular dynamics simulation in fully explicit solvent. The heating of the fully solvated complex to 1000 K during the simulated annealing protocol led to breaking of the complex observed by the number of intermolecular contacts falling to 0, but the complex would re-form during the simulation after the system cooled to 300 K (Supplementary Figure S2B).Therefore we concluded

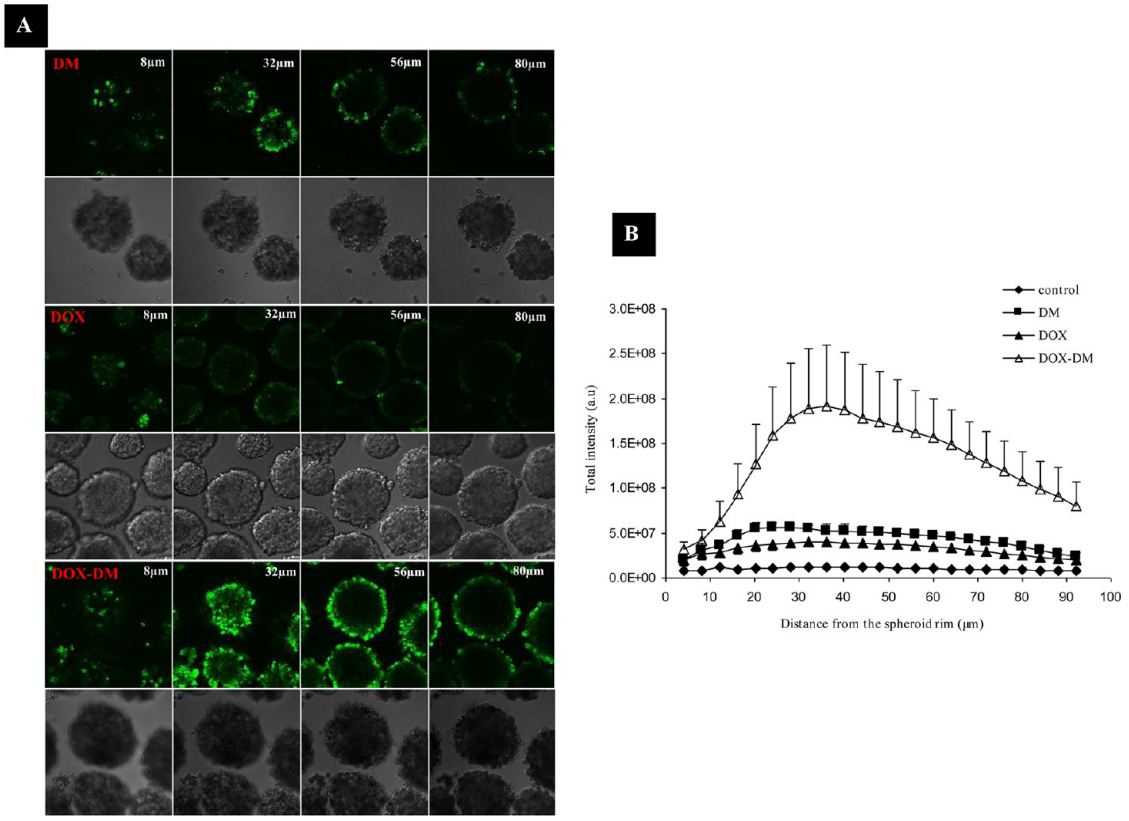

Figure 2. Penetration of DOX into prostate DU145 multicellular tumor spheroids (MTS). MTS were incubated with DM (100 μM), free DOX (10 μM), and DOX−DM (10 μM:100 μM equivalent to 1:10 molar ratio) for 1 h. (A) Optical MTS sections (4 μm) imaged by CLSM at 8, 32, 56, and 80 μm distance from the spheroid rim at 488 and 505 nm excitation and emission wavelengths respectively (20× lens). (B) Total intensity in each slice in the *z*-series was quantified, subtracted from the background, corrected for attenuation, and plotted *versus* distance from the spheroid rim (n = 5 MTS). DOX−DM signals showed at least an 8-fold increase compared to free DOX signals with a maximum at 40 μm depth. For quantification purposes, the MTS rim was considered to be the portion touching the coverslip.

that intermolecular complex of DOX and DM can be formed in solution by molecular modeling and ^{1}H NMR spectroscopy. The hydrogen-bonding and intermolecular interactions between the anthracycline ring of DOX and methylene groups of DM may be responsible for complex formation.

Enhanced Penetration and Retention of DOX−DM Complexes into Prostate MTS. MTS has increasingly become the most commonly used tool to assess drug penetration qualitatively and quantitatively by autoradiography or fluorescence microscopy. Herein, we assessed the penetration of DOX, in the free or complexed form (1:10 Dox:DM molar ratio), into DU145 prostate MTS, at a final DOX concentration of 10 μM. This concentration was sufficient to detect DOX signals by CLSM as reported before.[16] Histological examination of MTS was performed by H&E, which confirmed the presence of three layers: (i) a peripheral rim of proliferating cells, (ii) an inner shell of nonproliferating, quiescent cells, and (iii) a central core of necrotic cells (Supplementary Figure S3). DU145 MTS (200 ± 50 μm in diameter) were incubated for 1 h with free DOX and DOX−DM complexes; then the MTS were washed and visualized under CLSM. MTS were optically sectioned, and the total intensity in 4 μm thick sections was measured and plotted against the distance from the outer spheroid rim (section touching the coverslip). Our CLSM images showed that while DOX (Figure 2A, middle) was detected uniformly with low-intensity signals throughout the MTS sections, DOX−DM complexes (Figure 2A, bottom) penetrated as deep as 80 μm. Such a pattern was similar to the distribution of intrinsically fluorescent DM[13] (Figure 2A, top). Moreover, DOX−DM complexes showed 8- and 4-fold increases in DOX intensity signals at 40 and 80 μm depths, respectively (Figure 2B, open triangles). We concluded that complexation of DOX to the cationic DM improves its accumulation in the proliferating layer of the MTS.

DOX−DM Complexes Delayed MTS Growth *in Vitro*. One of the serious disadvantages of chemical conjugation of a drug to its carrier is the possibility of drug deactivation. Moreover, physical incorporation approach could suffer from the same problem but to a lesser degree. Therefore, it was essential to evaluate the DOX−DM cytotoxicity in both the DU145 monolayer and MTS before studying the DOX−DM effect on MTS growth. annexin V/PI staining confirmed that DOX−DM was cytotoxic to cells from both cultures (Figure 3 and

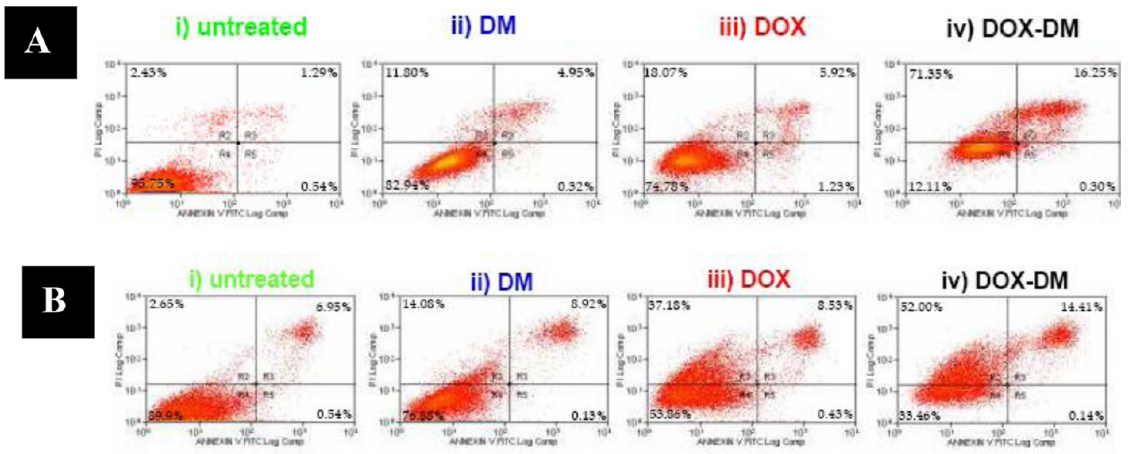

Figure 3. Assessment of DOX−DM complex cytotoxicity by annexin V/propidium iodide (PI) staining. DU145 monolayers (A) or MTS (B) were incubated with the test compounds: DOX (10 μM), DM (100 μM), or DOX−DM (10 μM DOX:100 μM DM equivalent to 1:10 molar ratio) for 1 h and allowed to recover for another 24 h. Cytotoxicity was assessed by annexin V and PI staining and quantified by flow cytometry. Two-dimensional flow cytometry histograms showing the percentages of unstained living population (bottom left quarter; annexin V-FITC$^-$/PI$^-$), apoptotic cells (bottom right quarter; annexin V-FITC$^+$/PI$^-$), late apoptotic cells (top left quarter; annexin V-FITC$^+$/PI$^+$), and cell debris (top left quarter; annexin V-FITC$^-$/PI$^+$).

Supplementary Figure S4). Furthermore, an enhanced toxicity of the complex was observed and clearly seen by the statistically significant ($p < 0.001$) reduction in the percentage cell viability in the monolayer and MTS cultures, respectively (Figure 3 and Supplementary Figure S4). This concludes that DOX complexation did not compromise its activity but showed an increase in its cytotoxicity, more evidently in the monolayer system. The enhanced toxicity could be a result of increased DOX concentration in the monolayer or in the outer proliferating layers of the MTS.

In order to examine whether the enhanced, deeper penetration and retention of DOX−DM complexes in MTS, as observed by CLSM (Figure 2), can potentiate DOX cytotoxicity and delay the MTS growth, we incubated DU145 MTS with free DOX (1 and 10 μM), DM (100 μM), or DOX−DM complexes (1:100 and 1:10) for 1 h (a single exposure). Then MTS were washed and their volume was monitored up to 21 days. Our results showed that DM alone (100 μM) had no effect on MTS growth (Figure 4B). Moreover, incubation with free DOX (10 μM) or DOX−DM (1:10) showed significant reduction in normalized MTS volume compared to untreated MTS ($p < 0.001$ on day 14 or 21) (Figure 4A). Since high DOX concentration (*i.e.*, 10 μM) was found to delay MTS volume significantly even after 1 h incubation, we lowered DOX concentration to 1 μM DOX, while keeping DM concentration the same (1:100 molar ratio). Interestingly, MTS incubated with low DOX concentration (1 μM) showed no reduction in volume compared to control MTS, while MTS treated with DOX:DM complexes (1 μM DOX, 1:100 molar ratio) clearly exhibited significantly smaller volumes compared to MTS treated with equivalent free DOX concentration (1 μM) ($p < 0.001$) particularly on days 14 and 21 (Figure 4B and C).

DOX−DM Retention into Calu-6 Tumor Xenograft Model *in Vivo*. In order to translate the findings obtained from the interaction of DOX−DM with the avascular *in vitro* tumor microenvironment model (MTS) to the vascularized and more complex *in vivo* solid tumor model, we conducted a study where the DOX−DM (1:10) complexes were injected into a Calu-6 xenograft model by direct intratumoral administration, and DOX fluorescence was monitored up to 24 h using an IVIS imaging system. Interestingly, complexation of DOX to the DM greatly enhanced its retention within the lung epithelial Calu-6 xenografts. Similar to the MTS results, DOX fluorescence was significantly higher in the DOX−DM-treated group compared to the free-DOX-treated group, especially at early time points of 0.5, 1, and 2 h. DOX−DM complex was still detected in the tumors even 24 h after administration (Figure 5A and B). Mice injected with DM alone in the absence of DOX showed no fluorescence *in vivo* at the dose studied, which indicated that the detected signals were due to DOX fluorescence alone (Supplementary Figure S8B). These results confirmed that complexation of DOX to DM increased DOX penetration and retention not only in MTS *in vitro* but also in human xenograft *in vivo*.

Tumor Growth Delay and Survival Studies in the Transplanted Syngeneic B16F10 Melanoma Model. To assess the therapeutic effect of the DOX−DM complex, a mouse syngeneic melanoma model was employed. C57/Bl6 mice bearing B16F10 mouse melanoma were treated with DOX (0.5 mg/kg), DM (50 mg/kg), or DOX−DM (0.5 mg/kg: 50 mg/kg) administered *via* intravenous route. The results of the tumor growth delay following different treatments are shown in Figure 6A. There was no significant therapeutic effect induced by DOX or DM alone compared to the control, untreated group under the conditions studied. In contrast, a single-dose injection of DOX−DM delayed

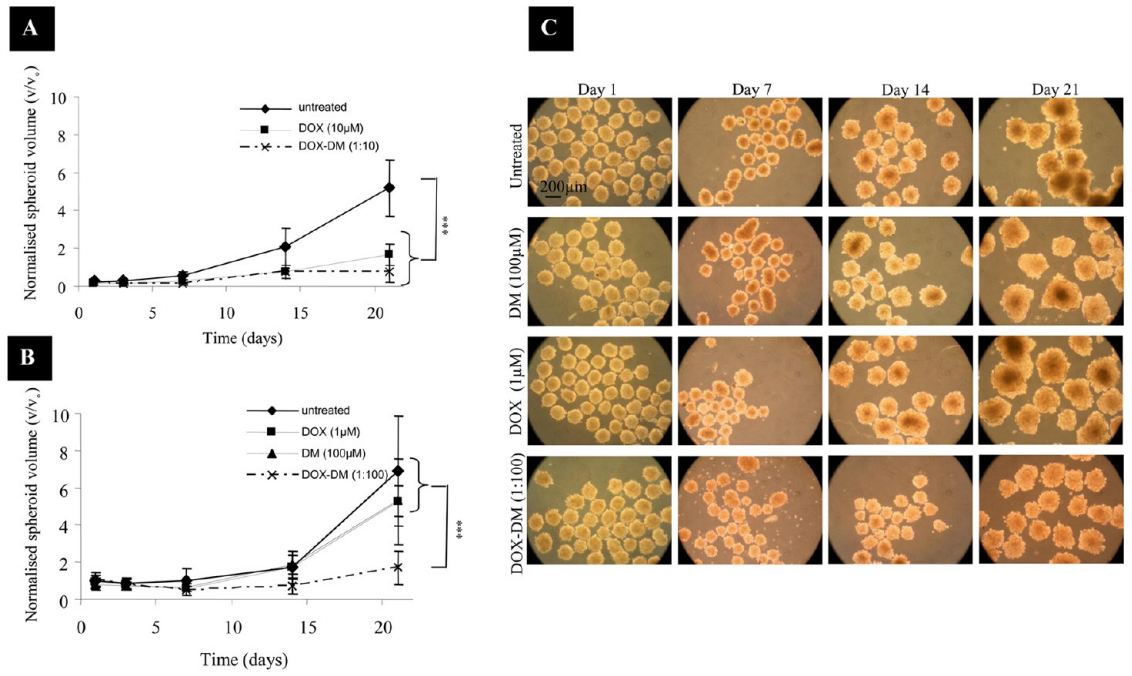

Figure 4. Growth curves of DU145 MTS before and after treatment with DOX−DM complexes. (A) Mean MTS volume (*V*) on the day of measurement was normalized to the initial volume (V_0) and plotted against days after exposure. MTS treated with DOX (10 μM) (free and complexed) showed significant volume reduction in comparison to untreated control (A). (B) MTS treated with low-concentration DOX (1 μM) complexed with DM (1:100) showed significantly delayed growth compared to all other treated groups on days 14 and 21 postexposure (*$p < 0.001$). (C) Photomicrographs of control MTS on days 1, 7, 14, and 21 after treatment with DM (100 μM), free DOX (1 μM), and DOX−DM (1 μM:100 μM). About 100 MTS were harvested from agar-coated 96-well plates on day 4 after seeding (0 day exposure) and incubated for 1 h with the test material, rinsed, and transferred to agar-coated plates in complete media. MTS were imaged using a Nikon camera attached to an Olympus microscope, and images were analyzed using ImageJ software (NIH, USA).**

tumor growth compared to all other groups, with statistical significance obtained on day 12 ($p < 0.01$) and day 13 ($p = 0.001$). In the survival study, animals were euthanized when the tumors became larger than 150 mm^2. Mice treated with DOX−DM complex displayed significantly prolonged median survival times compared to the untreated and free DOX groups ($p < 0.015$), but not the free DM group ($p < 0.04$) (Figure 6B). The median survival time for the group injected with DOX−DM complex was 16 days compared to 13 days for other treated and nontreated groups. No significant weight loss after treatment was observed in all the groups (data not shown).

CLSM was then carried out on frozen sections of B16F10 tumors at 1 h after i.v. injection in order to assess the DOX distribution pattern within the tumor mass. A higher dose of DOX was injected in this experiment compared to the therapy experiment (20 times higher) to facilitate detection of DOX fluorescence signals *in vivo*. Despite the presence of DOX in both DOX−DM and free-DOX-treated tumors, a clear difference in intratumoral DOX distribution pattern was observed (Supplementary Figure S9B). Cells treated with DOX alone exhibited better cell-to-cell contact, while tumors treated with DOX−DM demonstrated larger gaps between the cells. This result supports the hypothesis that DM enhanced DOX penetration wihin the tumor mass through loosening cell-to-cell contact, leading to enhanced inhibition of tumor growth and prolonged animal survival in the DOX−DM-treated group compared to the DOX-alone-treated group.

DISCUSSION

Lack of penetration of anticancer drugs into a tumor mass at a lethal concentration has increasingly become recognized as an important cause of cytotoxic drug resistance.[17] Both physicochemical properties of drugs (*i.e.*, molecular weight, charge, and solubility) and tumor physiology (*i.e.*, poorly formed vasculature, hypoxia, increased levels of intrafluid pressure, and high levels of P-glycoprotein expression) determine the rate of diffusion through tissues.[18] Previous studies with CLSM or flow cytometry have shown poor penetration of DOX into DU145 MTS,[9] PC-10 lung and HEp-2 MTS,[19] and V79 MTS[7] with fluorescence staining only in one or two outer layers of MTS, after 1−2 h exposure. Other studies carried out *in vivo* showed poor uptake, compared to other organs, and considerable variation of penetration into the tumor tissues.[12] Such studies proposed poor penetration as a major limitation in DOX chemotherapy. Experimental results with DOX consistently showed a correlation between limited penetration into MTS and the reduced activity against centrally located cells.[20,21]

Several strategies to enhance penetration of anthracyclines *in vitro* using the MTS system have been

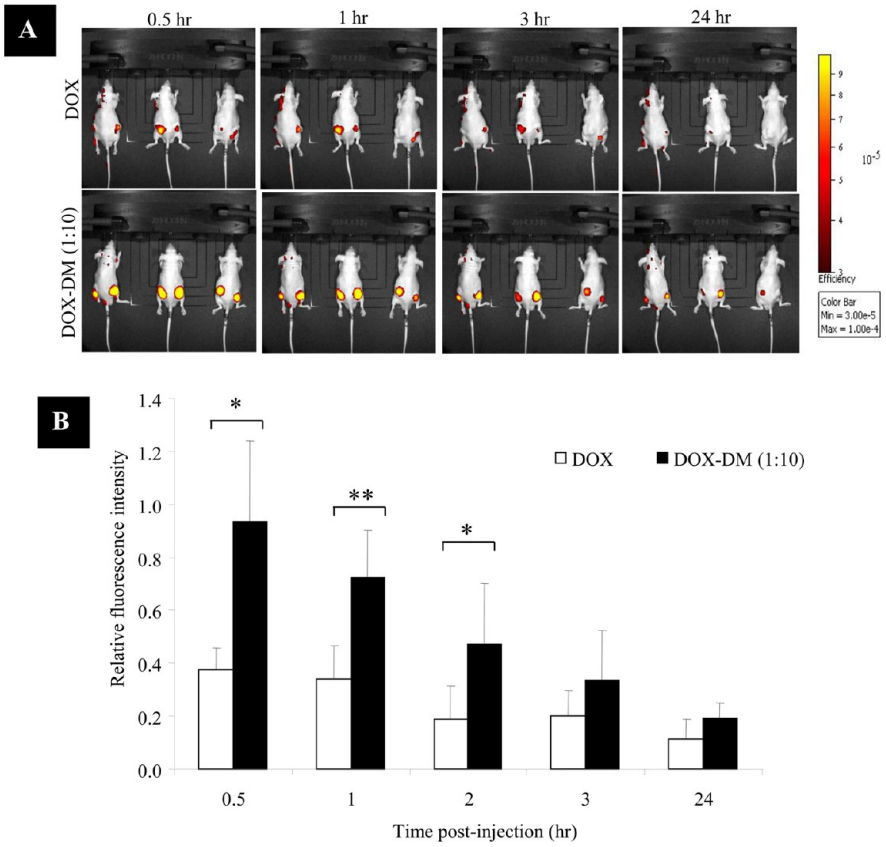

Figure 5. Retention of DOX−DM complexes within Calu-6 tumor xenografts shown by live fluorescence imaging. (A) Live fluorescence images of mice injected intratumorally with 50 μL containing DM, DOX (2.5 μg), or the complexes (1:10 molar ratio), captured at 0.5, 1, 2, 3, and 24 h postadministration at 5 s exposure. (B) Fluorescence intensity signals from the tumor (region of interest) were quantified and normalized to signals from the 5 min time point. Only xenografts treated with DOX−DM complexes showed significantly enhanced retention within the tumors at 0.5, 1, and 2 h postinjection compared to the free-DOX-treated group (*$p < 0.05$, **$p < 0.01$). Fluorescence signals of DOX−DM could be detected within the tumors up to 24 h postadministration. All images were captured using an IVIS lumina II imaging system.

reviewed.[22] This includes the use of lipophilic derivatives of DOX, coadministration of penetration enhancers such as Brij 30 in low doses, and incorporation into low-density lipoprotein. Others have been proposed such as preincubation with antiadhesive agents such as hyaluronidase[19] and facilitating its endosomal escape by the use of chloroquine[23] or omeprazole.[24] Another approach to improve DOX penetration into tumor tissues was encapsulation into liposomes[25] and the use of P-glycoprotein inhibitors.[26] Dendrimers constitute another class of drug delivery systems and have been proposed preclinically as drug delivery carriers of doxorubicin[27−30] and other anticancer drug such as methotrexate[3,31−33] and camptothecin.[4,34,35] Drug incorporation occurs either by covalent conjugation of drugs to the dendrimer surface functionalities or noncovalently *via* encapsulation of drugs within the dendritic structure. A combination of both surface and core interactions has been reported.[36] Approaches followed to improve intracellular uptake include targeting with ligands such as folic acid[37] or transferrin.[30]

Herein, we have employed an antiangiogenic polycationic PLL dendrimer to complex the poorly soluble cytotoxic drug DOX and improve its delivery into the proliferation cells of a three-dimensional prostate cancer (DU145) MTS model *in vitro*. This is the first study to examine systemic complexation between DOX and poly-L-lysine dendrimer with enhanced penetration and retention of the complex in a 3D MTS cancer model *in vitro*.

Our NMR results (Figure 1) suggested enhanced dispersilibity of DOX upon complexation to DM, so one might expect that dimerization of DOX is reduced, and thus better internalization into cells may occur. Furthermore, we have previously studied the intracellular fate of the PLL dendrimer employed here by confocal microscopy and have shown its ability to reach the nucleus within the first 15 min of incubation.[13] These previous results could explain the enhanced uptake of DOX observed in cells in our study. El-Sayed *et al.*[52] reported that cationic PAMAM dendrimers (G0−G4) reduced trans-epithelial electrical resistance measurements in Caco-2 culture, which is attributed to loosening the tight junctions between the cells in the culture. Similar findings were observed with our DM in Caco-2 culture (data not shown).

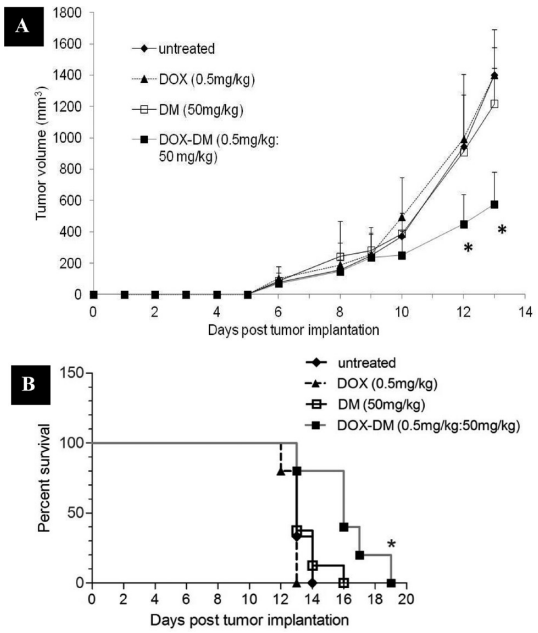

Figure 6. Tumor growth and survival curves after intravenous administration of DOX−DM complexes in the B16F10 melanoma model. (A) Growth curves of B16F10 tumors. B16F10 cells were inoculated under the skin of C57Bl6 mice, and a single injection of the therapy was carried out on day 8 post-tumor implantation. Animals were divided into four treatment groups: untreated, free DOX (0.5 mg/kg), free DM (50 mg/kg), and DOX−DM complex (0.5 mg/kg:50 mg/kg) groups. Results are shown as mean ± SD ($n = 7-10$ animals) (*$p < 0.05$). (B) Survival analysis of tumor-bearing mice treated as in (a).

Such results together with enhanced cellular uptake could partially explain the enhanced penetration of DOX in the MTS model.

It is worth mentioning that the same DOX and DM concentrations were used for the monolayer and MTS annexin V/PI cytotoxicity studies. However more synergy in cytotoxicity was seen in the case of the monolayer compared to the MTS system. Differences in toxicity between the monolayer and MTS could be due to a difference in the kinetics of penetration, as it is expected that diffusion of the drug would be much faster across one monolayer as opposed to a multilayer system, as in the case of MTS. The cytotoxicity assessment was done only 24 h postincubation, which might be a short period to observe synergistic cytotoxicity in the case of the MTS. This rationale could be supported by the fact that longer term monitoring of MTS growth has shown significant differences in size between the MTS treated with the complex and treatment with the free drug, which clearly suggests enhanced cytotoxicity in the case of the complex. Similar results were found by Walker *et al.*,[38] where the cytotoxicity of clinically important compounds such as doxorubicin and vinblastine was reduced in MCF7 MTS *versus* MCF7 monolayers. We therefore concluded that there was a correlation between drug retention (concentration) and delayed MTS growth (biological activity), indicating that the drug complex was biologically active.

Our results disagree with results obtained by Jain *et al.*, who showed no difference in cytotoxicity between free DOX and DOX encapsulated in nontargeted polypropyleneimine-based dendrimers when tested in an A549[39] and MCF7[40] cell monolayer system. However, the two dendrimers are chemically different. The DOX−DM complex not only has been delivered into the *in vitro* 3D cancer models but also showed significant enhancement in tumor retention up to 24 h in comparison to the free DOX. In this work, the complex was administered by direct intratumoral injection; however, we have previously shown that this dendrimer passively targets the solid tumor (~4% of injected dose per gram tissue), without any chemical modification, *i.e.*, PEGylation,[29,30,33] or active targeting[30,33] required.

Localization and retention of different anticancer drugs and delivery systems in the tumor mass by i.t. administration has been extensively studied. Many reports showed that the clearance rate from the tumor volume is highly dependent on the drug/nanoparticle molecular weight and surface charge. Nomura *et al.* studied the correlation between the particle size and surface charge and the retention in tissue-isolated tumors after intratumoral injection.[53] It was found that free drugs and zwitterionic delivery systems (emulsions and liposomes) around 100 nm in diameter were leaking from the tumor immediately after administration. On the other hand, positively charged particles with similar sizes significantly increased tumor injection retention.[54] These reports are in agreement with our DOX and DOX−DM findings following i.t. injection in Calu-6 xenografts.

In the current study, DOX was leaking immediately from the tumor following i.t. injection. On the other hand, positively charged DOX−DM complexes (Table S1) retained significantly higher DOX in the tumor up to 2 h. Between 3 and 24 h postinjection a gradual reduction in the fluorescence of DOX−DM complexes was observed. This reduction can be due to subsequent release of DOX from the DM, which can then be washed out *via* lymphatic drainage as the free DOX. Alternatively deeper penetration of these complexes in the tumor mass, thus limiting their detection by optical imaging, may have occurred. Further studies are warranted to understand the fate of these complexes *in vivo* using more sensitive and quantitative measurements such as using[14] C-DOX and liquid scintillation counting. Fluorescence analysis is not very reliable over extended periods of time since fluorescence properties (optical stability) of DOX were highly dependent on the surrounding environment (pH, ions, serum proteins). Future studies will focus on the mechanistic aspect of DOX behavior at the cellular and multicellular tumor level *in vitro* and *in vivo*.

The choice of this particular dendrimer in this study was based on two previous findings: (i) we have previously established that PLL-DM exhibits antiangiogenic activity comparable to Avastin in delaying B16F10 tumor growth *in vivo*. Numerous studies using anti-VEGF agents, such as bevacizumab (Avastin), have indicated that the addition of antiangiogenic therapeutics along with chemotherapy or radiotherapy can synergistically improve tumor responses to treatment. (ii) We have reported DM trafficking into the nucleus within 25–45 min of incubation with the cell monolayer *in vitro*,[13] so we propose that complexation of DOX to DM may offer synergistic therapeutic effect, enhanced accumulation in the tumor mass, and rapid shuttling of DOX molecules into the nucleus of tumor cells.

Many studies have been carried out to document the therapeutic efficacy of DOX incorporated within different dendritic polymers using *in vivo* animal tumor models. Zhu *et al*. have reported the use of two types of linkers (acid-sensitive and acid-insensitive) to couple DOX with partly PEGylated fourth-generation polyamidoamine dendrimers.[29] The conjugate with acid-sensitive linker displayed higher tumor accumulation, which favored its antitumor activity in the B16F10 mouse melanoma model. A different approach with a similar concept was reported by Calderón *et al*., where DOX was incorporated into a polyglycerol construct *via* an acid-sensitive linkage that was further coated with a PEG shell.[41] In the latter study, DOX used at a dose of 24 mg/kg led to complete remission for up to 30 days post tumor implantation. A recently published study was conducted with an attempt to compare a PEGylated generation 5 PLL dendrimer–DOX conjugate with the commercial PEGylated liposomal DOX formulation Caelyx using rat and mouse tumor models.[42] Such results showed that the dendrimer formulation exhibited improved therapeutic activity compared to the liposomal formulation and free DOX exhibited by the profound tumor growth inhibition and longer survival times achieved in the dendrimer–DOX group. It is worth mentioning that the dose of DOX injected in the three groups was not consistent with 4.5, 5, and 10 mg/kg DOX injected in free DOX, liposomal–DOX, and dendrimer–DOX groups, respectively.[42] The previous studies employed PEGylation to prolong blood circulation time of the dendrimer; in addition they utilized a multiple-administration approach. In the current study, only a single injection of DOX–DM complex was performed, and moreover an extremely low dose of DOX was utilized (0.5 mg/kg), in comparison to previous studies where DOX dose was higher than 4 mg/kg. The most important finding in this study was the significantly delayed tumor growth observed in the DOX–DM-treated group (on days 12 and 13) and the improved animal survival compared to all other treated groups. No significant weight loss was observed, unlike results obtained in the previous studies employing high DOX doses,[41,42] indicating the lack of DOX toxicity. It is worth mentioning here that we previously reported that intravenous injection of this particular dendrimer at 50 mg/kg/day (once daily) on days 1 and 2 post-tumor inoculation led to a delay in tumor growth. In this study (Figure 6), free DM did not exhibit any therapeutic effect. We attribute the difference in results obtained in Figure 6 and the previously reported work to the difference in the number of injections and timing of the therapy. Previously DM was injected on days 1 and 2 post-tumor implantation (to interfere with the angiogenesis process of the tumor), while in this work the DM was injected after the tumors had been fully vascularized (on day 8) and only a single injection (50 mg/kg) was given.

CONCLUSION

This study illustrated the complexation of doxorubicin with cationic poly-L-lysine dendrimer. The complex showed better penetrability into monolayers, the MTS system, and *in vivo* tumors than the free drug. There was a significant increase in toxicity of the drug upon complexation both *in vitro* and *in vivo*. Despite these encouraging results, more studies are still required to investigate the exact mechanism(s) behind the enhanced DOX toxicity *in vitro* and *in vivo* upon complexation with DM. Overall, the use of antiangiogenic dendrimer-based therapeutics could offer a rational design of combinatory therapeutics (*i.e.*, antiangiogenic and chemotherapeutic) in cancer therapy *in vivo*.

MATERIALS AND METHODS

Materials. DM was synthesized as we previously described.[5,13] Chemicals and solvents were obtained from Sigma-Aldrich (USA) and were used as received. RPMI-1640 media, fetal bovine serum (FBS), penicillin/streptomycin, trypsin/EDTA, and phosphate-buffered saline (PBS) were obtained from Gibco, Invitrogen (UK). Annexin-V-Fluos Staining Kit was purchased from Roche Diagnostics GmbH (Germany), and agar was from Bacto Agar (Detroit, MI, USA). Matrigel was purchased from Becton Dickinson (UK). SnakeSkin dialysis tubing (MWCO 3500 Da) was obtained from Fisher Scientific Ltd.

Spectrofluorimetry and Fluorescence Polarization. The emission spectra (200–900 nm) of DOX (17.2 μM), DM (0–344 μM), and DOX–DM complexed at 1:0, 1:0.5, 1:1, 1:2, 1:5, 1:10, and 1:20 molar ratios in PBS were obtained at a scan rate of 1200 nm/min in a 1 cm path length, in a 300 μL quartz cuvette (Hellma, Scientific Laboratory Supplies Ltd., UK) at 25 °C with 10 nm excitation and emission slit width, using a Perkin-Elmer luminescence spectrometer (LS 50B). All samples were excited using 499 nm wavelength light. DOX and DM stock solutions used were 3.4 mM and 736 μM, respectively. Area under the curve (AUC) was calculated between 518 and 800 nm. DOX fluorescence enhancement ratio upon complexation with DM was

expressed as

$$AUC_{DOX\ -\ DM}/(AUC_{DOX} + AUC_{DM})$$

In binding isotherm studies, the *G*-value was calculated using free DOX; then the FP value was measured for DOX−DM complexed at 1:0, 1:0.5, 1:1, 1:2, 1:5, and 1:10 using the same concentrations used in spectrofluorimetry studies. Each sample was measured over 5 min to obtain equilibrium conditions.

Molecular Modeling. The structures of DM and DOX for initial studies were generated using ChemBioOffice v.11 and saved as mol2 files. Structures were imported into Maestro v8.0, and further calculations were carried out using Macromodel 9.11[43] and the OPLS2005 force field as implemented in Macromodel (Cramer, 1995). The protonation states of both molecules were predicted using the LigPrep module of the Schrodinger software suite. The aqueous environment was taken into account using implicit solvent representation, namely, the generalized Born/surface area continuum (GB/SA) method,[44] with a constant dielectric function ($\varepsilon = 1$). An extended set of nonbonded cutoffs (van der Waals: 8 Å; electrostatics: 20 Å) was used. The modeling of the DM−DOX was carried using conformational search and Monte Carlo Mixture Model torsional sampling. DOX was positioned in two different starting configurations with respect to the initial model of DM, and 5000 steps of Monte Carlo conformational search were carried out for each configuration. The conformational search was carried out on a substructure consisting of one DM branch and DOX, while the rest of the DM was implicitly considered as a shell.

The DM was rebuilt using the protocol for generating 3D structures of hyperbranched molecules in sequence.[45] Molecular dynamics simulations were performed with Desmond version 3.03.1[46,47] using the OPLS2005 force field. All systems were simulated in the presence of explicit water molecules using the SPC model and a cubic box, with a size determined by a 10 Å buffer from molecules. The system was neutralized by addition of Cl^- ions. Molecular dynamics simulations were run in the NPT ensemble at 300 K and 1.01325 bar for 5000 ps. The default simulated annealing protocol consisting of 10 ps of heating to 10 K, 100 ps of heating to 100 K, 200 ps of heating to 300 K, 300 ps of heating to 1000 K, and 1000 ps of simulation at 300 K was run in the NVT ensemble. The systems were relaxed before all simulations by using the default Desmond protocol. The trajectories were generated by saving system snapshots every 5 ps, and energy values were recorded at 1 ps intervals.

NMR Spectroscopy. NMR spectra of DOX, DM, and complexes were acquired using a Bruker Avance spectrometer operating at a nominal ^1H frequency of 500 MHz and equipped with a 5 mm BBO probe including *z*-axis pulse field gradients. Spectra of samples in D_2O were acquired at 298 K and were processed using TOPSIN 1.3. Chemical shifts were referenced to the signal of sodium (trimethylsilane)-1-propanesulfonate at 0 ppm (^1H). Complexes were prepared as mentioned using deuterated water at final concentrations of 100 and 1000 μM for DOX and DM, respectively.

Culture of Cancerous Cell Lines. The DU145 prostate-tumor-derived cell line (DU145; ATCC, #HTB-81), Calu-6 human lung carcinoma (Calu-6; ATCC, #HTB-56), and B16F10 (ATCC, #CRL-6475) were cultured in RPMI-1640 supplemented with 10% FBS, 50 U/mL penicillin, 50 μg/mL streptomycin, 1% L-glutamine, and 1% nonessential amino acids, at 37 °C in 5% CO_2. Cells were routinely grown in 75 cm^2 canted-neck tissue culture flasks and passaged twice a week using trypsin/EDTA at 80% confluency.

Multicellular Tumor Spheroid Preparation. MTS consisting of the DU-145 cell line were prepared by the liquid overlay technique described by Yuhas *et al.*[48] In the MTS penetration study, approximately 2×10^6 cells, obtained by trypsinization from growing monolayer cultures, were seeded into 100 mm dishes coated with a thin layer of 1% agar in a total volume of 15 mL of culture media for 3−5 days to obtain MTS of 200 ± 50 μm in diameter, as observed under an inverted phase-contrast microscope with an ocular graticule. In cytotoxicity and growth delay experiments, MTS were cultured in 1% agar-coated nonadherent flat-bottomed 96-well plates at a seeding density of 12 500 cells/mL (0.2 mL/well) for 3−5 days.

DOX Penetration into DU145 MTS Study. Assessment of DOX penetration into MTS was performed as described previously in ref 16 with slight modifications. In brief, approximately 100 MTS were pooled on day 3−5 into a 15 mL conical base plastic tube and allowed to settle for 5 min. The bulk of the medium was then removed, leaving the MTS in the bottom of the tube, which were then transferred using a Pasteur pipet into an agar-coated six-well plate and incubated with 1 mL of serum-containing media consisting of DOX (10 μM), DM (100 μM), or DOX−DM (10 μM DOX:100 μM DM equivalent to 1:10 molar ratio) for 1 h at 37 °C and 5% CO_2 with intermittent agitation. MTS were then rinsed three times with PBS, transferred into a glass-bottom 24-well plate, and viewed using CLSM (Zeiss LSM 510 Meta; Carl Zeiss, Oberkochen, Germany) using a 30 mW 488 nm argon laser excitation source, a long-pass 505 nm output filter, and a Plan-Neofluar 20× lens to detect DOX fluorescence signals. Optical sectioning was confined to only 80 μm distance from the MTS rim due to fluorescence attenuation signals at greater depths.[16] For quantification purposes, the MTS rim was considered to be that touching the coverslip. In addition, cells within the MTS core consisted of quiescent nonproliferating cells arrested in the G0 phase of the cell cycle.[49] Excitation and emission wavelengths of DM are 453 and 514 nm, respectively, as previously described in ref 13.

To evaluate the depth of distribution of DOX or DOX−DM into the MTS, the optical probe technique described previously in ref 16 was used. In brief, radial recordings of total fluorescence intensity in a selected region of interest (ROI) were performed in MTS starting from the periphery (spheroid rim) toward the center (equatorial section). The pinhole settings of the confocal microscope were set to produce 4 μm thick sections and a whole *z*-series of 23 ROIs, allowing scanning until approximately 80−90 μm deep into the spheroid. For each spheroid image, the obtained total intensity was subtracted from background fluorescence obtained from untreated MTS, then corrected for the exponential light attenuation due to scattering and absorption within the spheroid. The linear attenuation coefficient was determined as described previously in ref 50 (see Supporting Information) and found to be 0.003165/μm. The total fluorescence intensity, after background subtraction and correction for scattering, was calculated in each ROI and plotted as a function of the distance from the spheroid rim. DM or DOX fluorescence was expressed in green.

Cytotoxicity Assessment in DU145 MTS and Monolayers. To assess the cytotoxicity of DOX (10 μM), DM (100 μM), or DOX−DM (10 μM DOX:100 μM DM equivalent to 1:10 molar ratio), MTS were treated in the same way as described in the penetration study and were prepared for flow cytometric analysis as described previously.[51] In brief, after the last rinsing step using PBS, MTS were trypsinized using 1 mL of trypsin-EDTA, and the MTS were incubated for 10 min at 37 °C using a Pasteur pipet, disintegrated into a single-cell suspension by gentle pipetting, and stained with annexin V and PI as per the manufacturer's instructions. A staining solution containing annexin V-FITC and PI was prepared immediately before cell staining: 20 μL of annexin V-FITC stain was combined with 20 μL of PI and made up with 1 mL of HEPES buffer solution. The solution was kept in the dark until added to resuspended cell pellets. DU145 monolayers were used as a control and incubated with the same concentrations of the drug as the MTS. Cell suspensions from either the monolayer or MTS were analyzed on a flow cytometer using 488 nm excitation and a 515 nm bandpass filter for fluorescein detection and a 615 nm filter for PI detection. Electronic compensation of the instrument was performed to exclude overlapping of the two emission spectra. Percentage of cell populations stained with annexin V-FITC, PI, or both was calculated to express cell viability.

Growth Delay Experiments in MTS. The biological activity of DOX and DM and the complex was tested by measuring the growth delay of the MTS after 1 h incubation with DOX (1 or 10 μM), DM (100 μM), or DOX−DM (1 or 10 μM DOX complexed with 100 μM DM). The MTS were then rinsed and reincubated in complete media and examined under an inverted microscope at 10× magnification, and photographs were taken with

subsequent size analysis using ImageJ/NIH software. MTS volume (V) was calculated using the following equation: $V = (4/3)\pi r^3$. The normalized volume was expressed as V/V_0 where V_0 is the volume on the day before starting treatment (day = 0 equivalent to day 4 from MTS seeding). MTS were measured three times weekly for the first week and then once weekly thereafter for 3 weeks. The media was changed twice a week.

Tumor Implantation. All animal experiments were performed in compliance with the U.K. Home Office Code of Practice for the Housing and Care of Animals Used in Scientific Procedures. In tumor uptake experiments, six- to eight-week-old female Swiss nude mice (Charles River Laboratories, UK) were caged in individually vented cages (Allentown, PA, USA) in groups of four with free access to food and water. A temperature of 19−22 °C was maintained, with a relative humidity of 45−65% and a 12 h light/dark cycle. The number of animals used in each group was 7−10. In therapy experiments, Swiss nude mice were substituted with C57Bl6 mice. Swiss nude mice were inoculated subcutaneously on the right and left flanks with 1×10^6 (50 μL) Calu-6 human epithelial lung carcinoma cells mixed with Matrigel (50 μL). C57Bl6 mice were inoculated subcutaneously on the right and left flanks with 1×10^6 (100 μL) B16F10 mouse melanoma cells suspended in PBS. The tumor volume was estimated by bilateral Vernier caliper measurement three to four times per week and calculated using the formula (width $\times$ width) $\times$ (length) $\times$ (π/6), where length was taken to be the longest diameter across the tumor. Intratumoral injections (imaging studies) were performed when the tumor volume reached 0.3−0.5 cm^3. Intravenous injections (therapy studies) were performed on day 8, when the tumor volume reached approximately 0.2−0.3 cm^3.

***In Vivo* Optical Fluorescence Imaging.** Live animal fluorescence optical imaging was used to monitor DOX retention *in vivo* of the fluorescent DOX using the IVIS Lumia II imaging system (Caliper Life Sciences Corp., Alameda, CA, USA). Images were acquired and analyzed using Living Image software 3.2 (Caliper Life Sciences Corp.). All images were acquired using the following settings: binning=4, exposure time=5 s, field of view=24, f-stop=2 and filters with an excitation of 500 nm and emission of 575−650 nm.

Data are displayed in the unitless value of efficiency and represent the ratio of light emitted to light incident. Mice were anesthetized using isofluorane and injected intratumorally with 50 μL containing DOX alone (2.5 μg) or the DOX−DM complex (1:10 molar ratio) as well as the equivalent dose of DM used in the complexes. All mixtures were prepared in 5% dextrose. The needle was inserted in the longitudinal direction from the tumor edge into the center of the tumor, 50 μL of the dispersion was administered slowly over 1 min, and the needle was left in the tumor for another 5 min to prevent sample leakage. Injections were carried out once for all groups. Fluorescence of DOX and DOX−DM was quantified prior to *in vivo* administration in a 96-well plate, to determine the sensitivity threshold for DOX fluorescence detection by IVIS (see Supporting Information).

***In Vivo* Tumor Growth Delay and Survival Studies.** To determine the therapeutic action of DOX *versus* DOX−DM complexes, B16F10 tumor bearing C57Bl6 mice were anesthetized using isoflurane and injected *via* tail vein with (i) DM at 50 mg/kg in 200 μL of 5% dextrose once on day 8, (ii) DOX at 0.5 mg/kg in 200 μL of 5% dextrose once on day 8, or (iii) DOX−DM complexes at 50 mg/kg DM complexed with 0.5 mg/kg DOX in 200 μL of 5% dextrose once on day 8 or (iv) left untreated. Mice were sacrificed by cervical dislocation when tumors reached 150 mm^2.

Statistical Analysis. Data are given as mean value ± SD, with n denoting the number of repeats. For differences in DOX retention in xenografts *in vivo*, one-tailed unpaired Student's t-test was applied. The survival curves between different groups were compared using the Kaplan−Meier method by GraphPad Prism V5.01. The statistical analysis was performed using the log-rank (Mantel−Cox) test, and the p values were later adjusted by the Bonferroni method. For all other experiments, significant differences were examined using one-way ANOVA. Tukey's multiple comparison test was further employed after one-way ANOVA for the tumor growth delay study. A p value of <0.05 was considered statistically significant in all studies.

Conflict of Interest: The authors declare no competing financial interest.

Acknowledgment. The authors would like to thank Dr. Parvinder Singh for advice on the cytotoxicity assay, Ms. Rima Karsan for help with ImageJ analysis, and Mr. Stephen Davison for MTS histological analysis (Department of Histopathology and Cytopathology, Royal Free Hospital). K.T.A.-J. is a recipient of the Maplethorpe Fellowship, The University of London. Partial funding from EPSRC (EP/G061998/1), BBSRC (BB/J008656/1), and the Royal Society is greatly acknowledged.

Supporting Information Available: This material is available free of charge *via* the Internet at http://pubs.acs.org.

REFERENCES AND NOTES

1. Tomalia, D. A.; Naylor, A. M.; Goddard, W. A. Starburst Dendrimers: Molecular-Level Control of Size, Shape, Surface Chemistry, Topology, and Flexibility from Atoms to Macroscopic Matter. *Angew. Chem., Int. Ed.* **1990**, *29*, 138–175.
2. Malik, N.; Evagorou, E. G.; Duncan, R. Dendrimer-Platinate: a Novel Approach to Cancer Chemotherapy. *Anticancer Drugs* **1999**, *10*, 767–776.
3. Kaminskas, L. M.; Kelly, B. D.; McLeod, V. M.; Boyd, B. J.; Krippner, G. Y.; Williams, E. D.; Porter, C. J. Pharmacokinetics and Tumor Disposition of PEGylated, Methotrexate Conjugated Poly-l-lysine Dendrimers. *Mol. Pharmaceutics* **2009**, *6*, 1190–1204.
4. Fox, M. E.; Guillaudeu, S.; Frechet, J. M.; Jerger, K.; Macaraeg, N.; Szoka, F. C. Synthesis and In Vivo Antitumor Efficacy of PEGylated Poly(l-lysine) Dendrimer-Camptothecin Conjugates. *Mol. Pharmaceutics* **2009**, *6*, 1562–1572.
5. Al-Jamal, K. T.; Al-Jamal, W. T.; Akerman, S.; Podesta, J. E.; Yilmazer, A.; Turton, J. A.; Bianco, A.; Vargesson, N.; Kanthou, C.; Florence, A. T.; *et al*. Systemic Antiangiogenic Activity of Cationic Poly-L-lysine Dendrimer Delays Tumor Growth. *Proc. Natl. Acad. Sci. U.S.A* **2010**, *107*, 3966–3971.
6. Hurwitz, H.; Fehrenbacher, L.; Novotny, W.; Cartwright, T.; Hainsworth, J.; Heim, W.; Berlin, J.; Baron, A.; Griffing, S.; Holmgren, E.; *et al*. Bevacizumab Plus Irinotecan, Fluorouracil, and Leucovorin for Metastatic Colorectal Cancer. *N. Engl. J. Med.* **2004**, *350*, 2335–2342.
7. Durand, R. E. Contributions of Flow Cytometry to Studies with Multicell Spheroids. *Methods Cell Biol.* **1994**, *42*, 405–422.
8. Kohno, T.; Matsutani, M.; Hoshino, T.; Takakura, K. Effects of Anticancer Drugs on Multicellular Spheroid of 9L Rat Brain Tumor. *No To Shinkei* **1985**, *37*, 991–997.
9. Wartenberg, M.; Acker, H. Induction of Cell Death by Doxorubicin in Multicellular Spheroids as Studied by Confocal Laser Scanning Microscopy. *Anticancer Res.* **1996**, *16*, 573–579.
10. Egorin, M. J.; Hildebrand, R. C.; Cimino, E. F.; Bachur, N. R. Cytofluorescence Localization of Adriamycin and Daunorubicin. *Cancer Res.* **1974**, *34*, 2243–2245.
11. Ozols, R. F.; Locker, G. Y.; Doroshow, J. H.; Grotzinger, K. R.; Myers, C. E.; Young, R. C. Pharmacokinetics of Adriamycin and Tissue Penetration in Murine Ovarian Cancer. *Cancer Res.* **1979**, *39*, 3209–3214.
12. Henneberry, H. P.; Aherne, G. W. Visualisation of Doxorubicin in Human and Animal Tissues and in Cell Cultures by Immunogold-Silver Staining. *Br. J. Cancer* **1992**, *65*, 82–86.
13. Al-Jamal, K. T.; Ruenraroengsak, P.; Hartell, N.; Florence, A. T. An Intrinsically Fluorescent Dendrimer as a Nanoprobe of Cell Transport. *J. Drug Target.* **2006**, *14*, 405–412.
14. Windsor, S. A.; Tinker, H. M. Binding of Biologically Important Molecules to DNA, Probed Using Electro-Fluorescence Polarization Spectroscopy. *Biophys. Chem.* **1996**, *58*, 141–150.
15. Zloh, M.; Ramaswamy, C.; Sakthivel, A.; Wilderspin, A.; Florence, A. F. Investigation of the Association and Flexibility of Cationic Lipidic Peptide Dendrons by NMR Spectroscopy. *Magn. Reson. Chem.* **2005**, *43*, 47–52.

16. Wartenberg, M.; Hescheler, J.; Acker, H.; Diedershagen, H.; Sauer, H. Doxorubicin Distribution in Multicellular Prostate Cancer Spheroids Evaluated by Confocal Laser Scanning Microscopy and the "Optical Probe Technique". *Cytometry* **1998**, *31*, 137–145.
17. Sutherland, R. M.; Eddy, H. A.; Bareham, B.; Reich, K.; Vanantwerp, D. Resistance to Adriamycin in Multicellular Spheroids. *Int. J. Radiat. Oncol. Biol. Phys.* **1979**, *5*, 1225–1230.
18. Jain, R. K. Vascular and Interstitial Barriers to Delivery of Therapeutic Agents in Tumors. *Cancer Metastasis Rev.* **1990**, *9*, 253–266.
19. Kohno, N.; Ohnuma, T.; Truog, P. Effects of Hyaluronidase on Doxorubicin Penetration into Squamous Carcinoma Multicellular Tumor Spheroids and Its Cell Lethality. *J. Cancer Res. Clin. Oncol.* **1994**, *120*, 293–297.
20. Erlanson, M.; Daniel-Szolgay, E.; Carlsson, J. Relations between the Penetration, Binding and Average Concentration of Cytostatic Drugs in Human Tumour Spheroids. *Cancer Chemother. Pharmacol.* **1992**, *29*, 343–353.
21. Erlichman, C.; Vidgen, D. Cytotoxicity of Adriamycin in MGH-U1 Cells Grown as Monolayer Cultures, Spheroids, and Xenografts in Immune-Deprived Mice. *Cancer Res.* **1984**, *44*, 5369–5375.
22. Kerr, D. J.; Kaye, S. B. Aspects of Cytotoxic Drug Penetration, with Particular Reference to Anthracyclines. *Cancer Chemother. Pharmacol.* **1987**, *19*, 1–5.
23. Poole, B.; Ohkuma, S. Effect of Weak Bases on the Intralysosomal pH in Mouse Peritoneal Macrophages. *J. Cell Biol.* **1981**, *90*, 665–669.
24. Mattsson, J. P.; Vaananen, K.; Wallmark, B.; Lorentzon, P. Omeprazole and Bafilomycin, Two Proton Pump Inhibitors: Differentiation of Their Effects on Gastric, Kidney and Bone H(+)-Translocating ATPases. *Biochim. Biophys. Acta* **1991**, *1065*, 261–268.
25. Vail, D. M.; Amantea, M. A.; Colbern, G. T.; Martin, F. J.; Hilger, R. A.; Working, P. K. Pegylated Liposomal Doxorubicin: Proof of Principle Using Preclinical Animal Models and Pharmacokinetic Studies. *Semin. Oncol.* **2004**, *31*, 16–35.
26. Martin, C.; Walker, J.; Rothnie, A.; Callaghan, R. The Expression of P-Glycoprotein Does Influence the Distribution of Novel Fluorescent Compounds in Solid Tumour Models. *Br. J. Cancer* **2003**, *89*, 1581–1589.
27. He, H.; Li, Y.; Jia, X. R.; Du, J.; Ying, X.; Lu, W. L.; Lou, J. N.; Wei, Y. PEGylated Poly(amidoamine) Dendrimer-Based Dual-Targeting Carrier for Treating Brain Tumors. *Biomaterials* **2011**, *32*, 478–487.
28. Lee, C. C.; Gillies, E. R.; Fox, M. E.; Guillaudeu, S. J.; Frechet, J. M.; Dy, E. E.; Szoka, F. C. A Single Dose of Doxorubicin-Functionalized Bow-Tie Dendrimer Cures Mice Bearing C-26 Colon Carcinomas. *Proc. Natl. Acad. Sci. U.S.A* **2006**, *103*, 16649–16654.
29. Zhu, S.; Hong, M.; Tang, G.; Qian, L.; Lin, J.; Jiang, Y.; Pei, Y. Partly PEGylated Polyamidoamine Dendrimer for Tumor-Selective Targeting of Doxorubicin: the Effects of PEGylation Degree and Drug Conjugation Style. *Biomaterials* **2010**, *31*, 1360–1371.
30. Han, L.; Huang, R.; Liu, S.; Huang, S.; Jiang, C. Peptide-Conjugated PAMAM for Targeted Doxorubicin Delivery to Transferrin Receptor Overexpressed Tumors. *Mol. Pharmaceutics* **2010**, *7*, 2156–2165.
31. Zhang, Y.; Thomas, T. P.; Desai, A.; Zong, H.; Leroueil, P. R.; Majoros, I. J.; Baker, J. R. Targeted Dendrimeric Anticancer Prodrug: A Methotrexate-Folic Acid-Poly(amidoamine) Conjugate and a Novel, Rapid, "One Pot" Synthetic Approach. *Bioconjugate Chem.* **2010**, *21*, 489–495.
32. Shukla, R.; Thomas, T. P.; Desai, A. M.; Kotlyar, A.; Park, S. J.; Baker, J. R. HER2 Specific Delivery of Methotrexate by Dendrimer Conjugated anti-HER2 mAb. *Nanotechnology* **2008**, *19*, 295102.
33. Jiang, Y. Y.; Tang, G. T.; Zhang, L. H.; Kong, S. Y.; Zhu, S. J.; Pei, Y. Y. PEGylated PAMAM Dendrimers as a Potential Drug Delivery Carrier: In Vitro and in Vivo Comparative Evaluation of Covalently Conjugated Drug and Non-covalent Drug Inclusion Complex. *J. Drug Target.* **2010**, *18*, 389–403.
34. Thiagarajan, G.; Ray, A.; Malugin, A.; Ghandehari, H. PAMAM-Camptothecin Conjugate Inhibits Proliferation and Induces Nuclear Fragmentation in Colorectal Carcinoma Cells. *Pharm. Res.* **2010**, *27*, 2307–2316.
35. Morgan, M. T.; Nakanishi, Y.; Kroll, D. J.; Griset, A. P.; Carnahan, M. A.; Wathier, M.; Oberlies, N. H.; Manikumar, G.; Wani, M. C.; Grinstaff, M. W. Dendrimer-Encapsulated Camptothecins: Increased Solubility, Cellular Uptake, and Cellular Retention Affords Enhanced Anticancer Activity in Vitro. *Cancer Res.* **2006**, *66*, 11913–11921.
36. Chauhan, A. S.; Sridevi, S.; Chalasani, K. B.; Jain, A. K.; Jain, S. K.; Jain, N. K.; Diwan, P. V. Dendrimer-Mediated Transdermal Delivery: Enhanced Bioavailability of Indomethacin. *J. Controlled Release* **2003**, *90*), 335–343.
37. Choi, S. K.; Thomas, T.; Li, M. H.; Kotlyar, A.; Desai, A.; Baker, J. R., Jr. Light-Controlled Release of Caged Doxorubicin from Folate Receptor-Targeting PAMAM Dendrimer Nanoconjugate. *Chem. Commun. (Cambridge, U.K.)* **2010**, *46*, 2632–2634.
38. Walker, J.; Martin, C.; Callaghan, R. Inhibition of P-Glycoprotein Function by XR9576 in a Solid Tumour Model Can Restore Anticancer Drug Efficacy. *Eur. J. Cancer* **2004**, *40*, 594–605.
39. Agarwal, A.; Gupta, U.; Asthana, A.; Jain, N. K. Dextran Conjugated Dendritic Nanoconstructs as Potential Vectors for Anti-Cancer Agent. *Biomaterials* **2009**, *30*, 3588–3596.
40. Gupta, U.; Dwivedi, S. K.; Bid, H. K.; Konwar, R.; Jain, N. K. Ligand Anchored Dendrimers Based Nanoconstructs for Effective Targeting to Cancer Cells. *Int. J. Pharm.* **2010**, *393*, 185–196.
41. Calderon, M.; Welker, P.; Licha, K.; Fichtner, I.; Graeser, R.; Haag, R.; Kratz, F. Development of Efficient Acid Cleavable Multifunctional Prodrugs Derived from Dendritic Polyglycerol with a Poly(ethylene glycol) Shell. *J. Controlled Release* **2011**, *151*, 295–301.
42. Kaminskas, L. M.; McLeod, V. M.; Kelly, B. D.; Cullinane, C.; Sberna, G.; Williamson, M.; Boyd, B. J.; Owen, D. J.; Porter, C. J. Doxorubicin-Conjugated PEGylated Dendrimers Show Similar Tumoricidal Activity but Lower Systemic Toxicity When Compared to PEGylated Liposome and Solution Formulations in Mouse and Rat Tumor Models. *Mol. Pharm.* **2012**, *9*, 422–432.
43. Mohamadi, F.; Richards, N.; Guida, W.; Liskamp, R.; Lipton, M.; Caulfield, C.; Chang, G.; Hendrickson, T.; Still, W. Macromodel—An Integrated Software System for Modeling Organic and Bioorganic Molecules Using Molecular Mechanics. *J. Comput. Chem.* **1990**, *11*, 440–467.
44. Still, W.; Tempczyk, A.; Hawley, R. C.; Hendrickson, T. Semianalytical Treatment of Solvation for Molecular Mechanics and Dynamics. *J. Am. Chem. Soc.* **1990**, *112*, 6127–6129.
45. Barata, T.; Brocchini, S.; Teo, I.; Shaunak, S.; Zloh, M. From Sequence to 3D Structure of Hyperbranched Molecules: Application to Surface Modified PAMAM Dendrimers. *J. Mol. Model.* **2011**, *17*, 2741–2749.
46. Lippert, R. A. A Common Avoidable Source of Error in Molecular Dynamics Integrators. *J. Chem. Phys.* **2007**, *126*, 046101–046102.
47. Bowers, K. J.; Dror, R. O.; Shaw, D. E. The Midpoint Method for Parallelization of Particle Simulations. *J. Chem. Phys.* **2006**, *124*, 184109–184111.
48. Yuhas, J. M.; Li, A. P.; Martinez, A. O.; Ladman, A. J. A Simplified Method for Production and Growth of Multicellular Tumor Spheroids. *Cancer Res.* **1977**, *37*, 3639–3643.
49. Haji-Karim, M.; Carlsson, J. Proliferation and Viability in Cellular Spheroids of Human Origin. *Cancer Res.* **1978**, *38*, 1457–1464.
50. Ballangrud, A. M.; Yang, W. H.; Charlton, D. E.; McDevitt, M. R.; Hamacher, K. A.; Panageas, K. S.; Ma, D.; Bander, N. H.; Scheinberg, D. A.; Sgouros, G. Response of LNCaP Spheroids after Treatment with an Alpha-Particle Emitter (213 Bi)-Labeled Anti-Prostate-Specific Membrane Antigen Antibody (J591). *Cancer Res.* **2001**, *61*, 2008–2014.

51. Terry, J.; Lubieniecka, J. M.; Kwan, W.; Liu, S.; Nielsen, T. O. Hsp90 Inhibitor 17-Allylamino-17-demethoxygeldanamycin Prevents Synovial Sarcoma Proliferation via Apoptosis in in Vitro Models. *Clin. Cancer Res.* **2005**, *11*, 5631–5638.
52. El-Sayed, M.; Ginski, M.; Rhodes, C.; Ghandehari, H. Transepithelial Transport of Poly(amidoamine) Dendrimers across Caco-2 Cell Monolayers. *J. Controlled Release* **2002**, *81*, 355–365.
53. Nomura, T.; Koreeda, N.; Yamashita, F.; Takakura, Y.; Hashida, M. Effect of Particle Size and Charge on the Disposition of Lipid Carriers after Intratumoral Injection into Tissue-Isolated Tumors. *Pharm. Res.* **1998**, *15*, 128–132.
54. Nomura, T.; Saikawa, A.; Morita, S.; Sakaeda Kakutani, T.; Yamashita, F.; Honda, K.; Takakura, Y.; Hashida, M. Pharmacokinetic Characteristics and Therapeutic Effects of Mitomycin C-Dextran Conjugates after Intratumoural Injection. *J. Controlled Release* **1998**, *52*, 239–252.